The reflected (M_{R1}) and transmitted (M_{T1}) signals are measured normalized to the reference signal. The unknown is then turned around to measure M_{R2} and M_{T2}. The scattering parameters of the device under test are given by the following equation system:

$$M_{R1} = e_{00} + \frac{s_{11}e_{01}(1 - s_{22}e_{22}) + s_{21}s_{12}e_{22}e_{01}}{D_1} \quad (1)$$

$$M_{T1} = e_{30} + \frac{s_{21}e_{32}}{D_1} \quad (2)$$

$$M_{T2} = e_{30} + \frac{s_{12}e_{32}}{D_2} \quad (3)$$

$$M_{R2} = e_{00} + \frac{s_{22}e_{01}(1 - s_{11}e_{22}) + s_{21}s_{12}e_{22}e_{01}}{D_2} \quad (4)$$

where

$$D_1 = 1 - s_{11}e_{11} - s_{22}e_{22} - s_{12}s_{21}e_{11}e_{22} + s_{22}s_{11}e_{11}e_{22} \quad (5)$$

$$D_2 = 1 - s_{22}e_{11} - s_{11}e_{22} - s_{12}s_{21}e_{11}e_{22} + s_{22}s_{11}e_{11}e_{22}. \quad (6)$$

As mentioned in [2], an iterative process can be used to find the scattering matrix of the unknown device. This has been found to be unnecessary since, by making substitutions in (1)–(4), the explicit solution has been found:

$$s_{11} = [C(1 + De_{11}) - ABe_{22}]/N \quad (7)$$

$$s_{12} = [1 + C(e_{11} - e_{22})]A/N \quad (8)$$

$$s_{21} = [1 + D(e_{11} - e_{22})]B/N \quad (9)$$

$$s_{22} = [D(1 + Ce_{11}) - ABe_{22}]/N \quad (10)$$

where

$$N = (1 + De_{11})(1 + Ce_{11}) - ABe_{22}^2 \quad (11)$$

$$A = (M_{T2} - e_{30})/e_{32} \quad (12)$$

$$B = (M_{T1} - e_{30})/e_{32} \quad (13)$$

$$C = (M_{R1} - e_{00})/e_{01} \quad (14)$$

$$D = (M_{R2} - e_{00})/e_{01}. \quad (15)$$

The scattering parameters of the unknown have to be determined at every frequency. Thus the explicit solution will save a lot of computer time.

When the coaxial switch S_a in Fig. 1 is included in the test unit, the measured device does not have to be manually turned during measurements. A flowgraph model for this system has been presented by Hackborn [1]. An explicit solution for the scattering parameters of the unknown has been found by Kruppa and Sodomsky [4].

In the flowgraph model by Hackborn, however, no leakage path is included. A flowgraph model including leakage paths is suggested in Fig. 3. Signals without parentheses apply when the switch S_a in Fig. 1 is in the left position, while signals in parentheses apply when the switch S_a is in the right position.

Again, by making measurements on standards, the error parameters r_{00}–r_{33} can be determined. The procedure will be similar to the one mentioned previously. The calibration process described by Hackborn [1] has to be extended to include two transmission measurements with $s_{12} = s_{21} = 0$ for the determination of r_{30} and r_{03}.

An analysis of the flowgraph yields

$$M_{R1} = r_{00} + \frac{s_{11}r_{01}r_{10}(1 - s_{22}r_{22}) + s_{21}s_{12}r_{22}r_{01}r_{10}}{D_3} \quad (16)$$

$$M_{T1} = r_{30} + \frac{s_{21}r_{32}r_{10}}{D_3} \quad (17)$$

$$M_{R2} = r_{33} + \frac{s_{22}r_{32}r_{23}(1 - s_{11}r_{11}) + s_{21}s_{12}r_{11}r_{32}r_{23}}{D_3} \quad (18)$$

$$M_{T2} = r_{03} + \frac{s_{12}r_{23}r_{01}}{D_3} \quad (19)$$

where

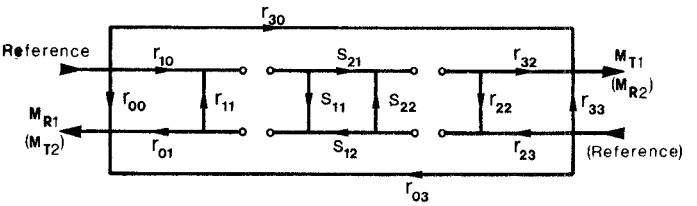

Fig. 3. Signal flowgraph of system model (switch S_a included in test unit).

$$D_3 = 1 - s_{11}r_{11} - s_{22}r_{22} - s_{12}s_{21}r_{11}r_{22} + s_{22}s_{11}r_{11}r_{22}. \quad (20)$$

The explicit solution to the scattering parameters of the measured device is then

$$s_{11} = [G(1 + r_{22}H) - r_{22}EF]/N_1 \quad (21)$$

$$s_{12} = E/N_1 \quad (22)$$

$$s_{21} = F/N_1 \quad (23)$$

$$s_{22} = [H(1 + r_{11}G) - r_{11}EF]/N_1 \quad (24)$$

where

$$N_1 = (1 + r_{11}G)(1 + r_{22}H) - r_{11}r_{22}EF \quad (25)$$

$$E = \frac{M_{T2} - r_{03}}{r_{01}r_{23}} \quad (26)$$

$$F = \frac{M_{T1} - r_{30}}{r_{10}r_{32}} \quad (27)$$

$$G = \frac{M_{R1} - r_{00}}{r_{01}r_{10}} \quad (28)$$

$$H = \frac{M_{R2} - r_{33}}{r_{23}r_{32}}. \quad (29)$$

As is seen above, the leakage paths will not significantly increase the computer time needed. Accuracy, however, will be improved.

ACKNOWLEDGMENT

The author wishes to thank Prof. E. F. Bolinder, Division of Network Theory, Chalmers University of Technology, Göteborg, Sweden, for his assistance and encouragement.

REFERENCES

[1] R. A. Hackborn, "An automatic network analyzer system," *Microwave J.*, pp. 45–52, May 1968.
[2] B. P. Hand, "Developing accuracy specifications for automatic network analyzer systems," *Hewlett-Packard J.*, pp. 16–19, Feb. 1970.
[3] H. V. Shurmer, "Calibration procedure for computer-corrected s parameter characterisation of devices mounted in microstrip," *Electron. Lett.*, pp. 323–324, July 12, 1973.
[4] W. Kruppa and K. F. Sodomsky, "An explicit solution for the scattering parameters of a linear two-port measured with an imperfect test set," *IEEE Trans. Microwave Theory Tech.* (Corresp.), vol. MTT-19, pp. 122–123, Jan. 1971.

Design of Optimum Acoustic Surface Wave Delay Lines at Microwave Frequencies

ANDREW J. SLOBODNIK, JR., MEMBER, IEEE, AND THOMAS L. SZABO, MEMBER, IEEE

***Abstract*—Optimum procedures for designing microwave acoustic surface wave delay lines are given. Combined beam steering diffraction loss curves are provided as a function of the basic material parameter, the slope of the power flow angle, to allow optimum**

Manuscript received June 28, 1973; revised September 4, 1973.
The authors are with the Air Force Cambridge Research Laboratories, Laurence G. Hanscom Field, Bedford, Mass. 01730.

choice of material for a given application. Methods for designing uniform periodic interdigital transducers including finger ohmic loss, lossy tuning elements, and parasitic capacitance have been extended to account for beam steering and diffraction.

I. INTRODUCTION

For a particular center frequency and time delay, the design of acoustic surface wave delay lines and other signal processing devices consists of optimizing the insertion-loss bandwidth product consistent with given system requirements. This, in turn, requires optimum specification of all design parameters including choice of material, interdigital transducer finger overlap (or acoustic aperture), and the number of interdigital periods.

The choice of the optimum material is generally undertaken first and depends on velocity, coupling constant [1], temperature coefficient of delay [2], [3], propagation loss [4]–[6], beam steering [7], and diffraction [8], [9]. The latter three properties become particularly important in the upper UHF and microwave frequency regions.

Quantitative data exist for each of the parameters listed above except for combined beam steering *and* diffraction loss. The purpose of this short paper is to provide such information. Since this loss is not simply the sum of its separate constituents, design curves must be more specific than the universal information possible when each loss mechanism is considered individually [8]. The aim of presenting these data is to enable the designer to: a) make an initial choice of material; b) determine when these loss mechanisms (which are external to the transducer) become significant; and c) pinpoint those variables that must be held to within specified tolerances in order to maintain acceptable loss levels.

The final sections of this short paper will outline procedures (with illustrative examples) for the design of optimum periodic unapodized acoustic surface wave delay lines at microwave frequencies. Transducer ohmic loss, lossy tuning inductor, parasitic capacitance, and beam steering and diffraction are all included along with the standard transducer design procedure. In other words, previous design optimization procedures [10]–[14] for uniform periodic interdigital transducers have been extended to account for beam steering and diffraction.

II. MATERIAL SELECTION INCLUDING DIFFRACTION AND BEAM STEERING

Diffraction is a fixed physical phenomenon for a given material, while beam steering (see Fig. 1) can be controlled by precise X-ray alignment at the expense of increased device cost. Both, however, influence the choice of acoustic surface wave substrate. An example of how the combined loss of beam steering and diffraction varies among materials is illustrated in Fig. 2, where the loss is given as a function of $\gamma = \partial\phi/\partial\theta$, the slope of the power flow angle [8]. As in all other cases in this short paper, loss has been calculated by integrating the complex acoustic amplitude over the aperture of the receiving transducer using the parabolic anisotropic diffraction theory [8] for identical unapodized input and output transducers. This theory has been explained in detail elsewhere [8] and its limits of applicability fully delineated [8]. Some popular orientations including YZ $LiNbO_3$ fall outside these limits.

For Fig. 2, the acoustic aperture is $\hat{L} = 80$ wavelengths, the distance between input and output transducers is $\hat{Z} = 5000$ wavelengths, and the misalignment from the desired pure mode axis, or the beam steering (BS) angle, is BS $\measuredangle = 0.1°$. In order to use these data for practical situations, it is only necessary to insert the slope of the power flow angle appropriate to the type and cut under consideration. It is also useful to note that

$$\hat{Z} = tf \tag{1}$$

where t is the time delay and f the frequency of the device of interest.

Several important features can be noted with reference to Fig. 2. Diffraction loss goes to 0 for those materials having $\gamma = -1.0$ and, as expected, the combined loss curve agrees exactly with the beam steering loss curve. Those materials having $\gamma = 0$ correspond to locally isotropic cases and beam steering goes to 0. Here, diffraction accounts for the total loss. Diffraction loss alone is symmetric about $\gamma = -1.0$ and beam steering loss about $\gamma = 0$, while the combined curve is clearly nonsymmetric.

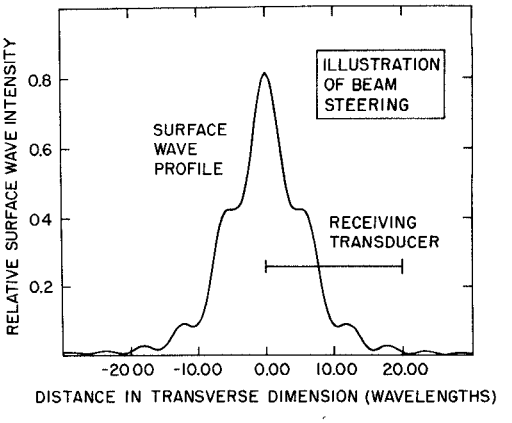

Fig. 1. Schematic of beam steering and diffraction: nonrectangular shape of surface wave profile is due to diffraction. Profile is not centered on receiving transducer due to beam steering. Both effects contribute to insertion loss when surface wave amplitude is integrated over receiving transducer.

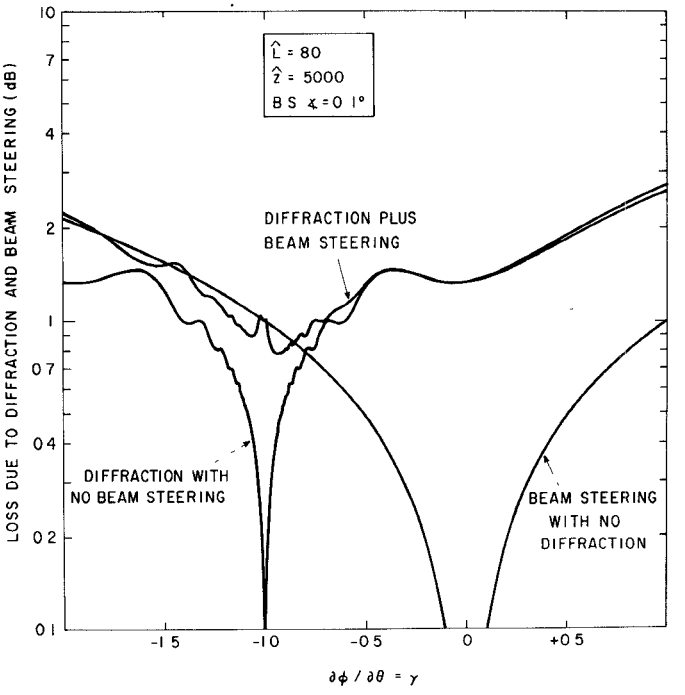

Fig. 2. Loss due to diffraction and beam steering as a function of slope of power flow angle for parabolic materials. $\hat{L}$ represents width of transducers in wavelengths. $\hat{Z}$ the distance between transducers in wavelengths. and BS $\measuredangle$ the beam steering angle.

The results illustrated in Fig. 2 are of major importance in choosing a material for a particular application. For example, where diffraction is potentially a very serious problem, as in highly apodized filters, a material having $\gamma \approx -1.0$ would be most desirable [15].

The importance of the beam steering angle is illustrated in Fig. 3 in which the combined loss curve of Fig. 2 is repeated along with two other curves for different beam steering conditions. From Fig. 3 it is evident that whenever beam steering angles are expected to be moderate or large, as, for example, in mass-produced devices where cost limits X-ray alignment precision, a material having $\gamma \approx 0$ should be chosen. Fig. 3 also shows by means of the drastic changes in the shapes of the curves that universal beam steering diffraction loss curves are not possible. This same point is illustrated in Fig. 4, which also yields some practical loss data for ST quartz [2] ($\gamma = +0.378$) and 001, 110 $Bi_{12}GeO_{20}$ ($\gamma = -0.304$). The *shape* of the $\gamma = -0.304$, BS $\measuredangle = 1.0$ curve is clearly different from that of the $\gamma = -0.304$, BS $\measuredangle = 0.0$ curve, and thus they could not be combined or superimposed.

Fig. 5 illustrates combined beam steering and diffraction loss versus the time-delay-frequency parameter $\hat{Z}$. These are the final

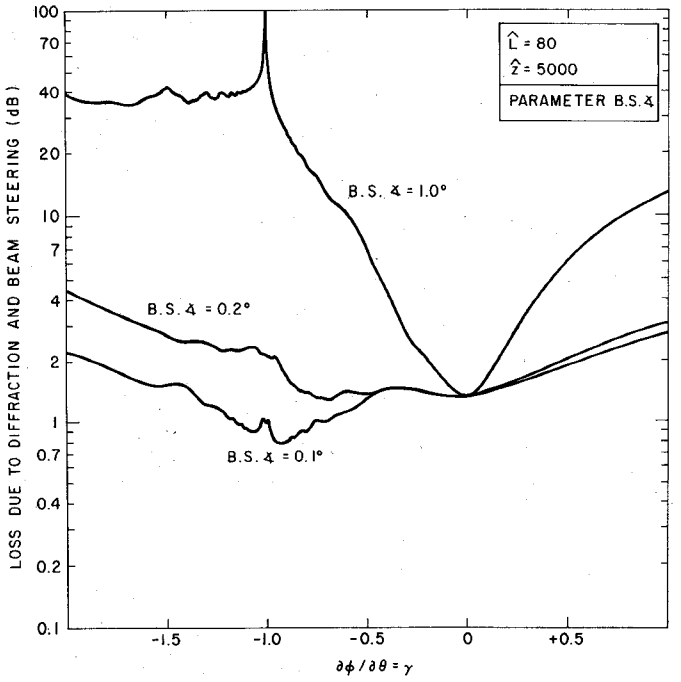

Fig. 3. Loss due to diffraction and beam steering as a function of slope of power flow angle with beam steering angle as parameter. Beam steering angle is defined as misalignment of center line between transducers from desired pure mode axis.

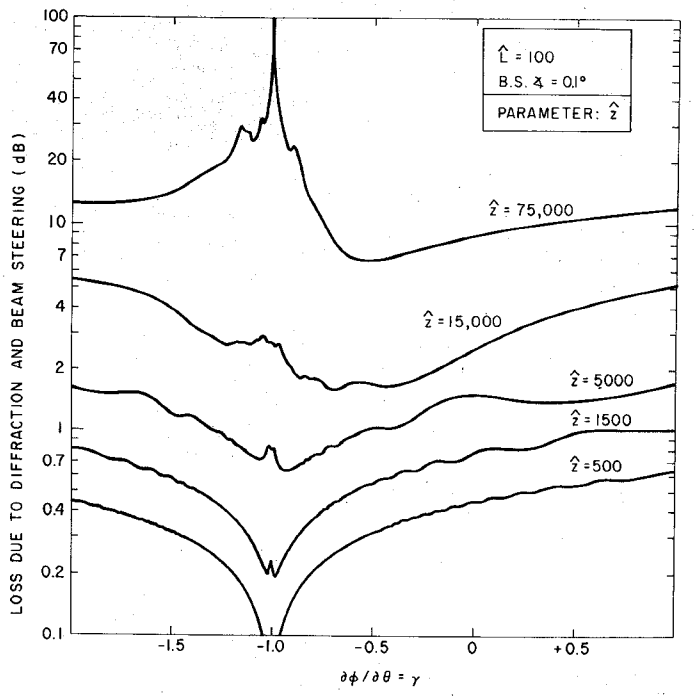

Fig. 5. Loss due to diffraction and beam steering as a function of slope of power flow angle with distance in wavelengths between transducers. $\hat{Z}$ as parameter.

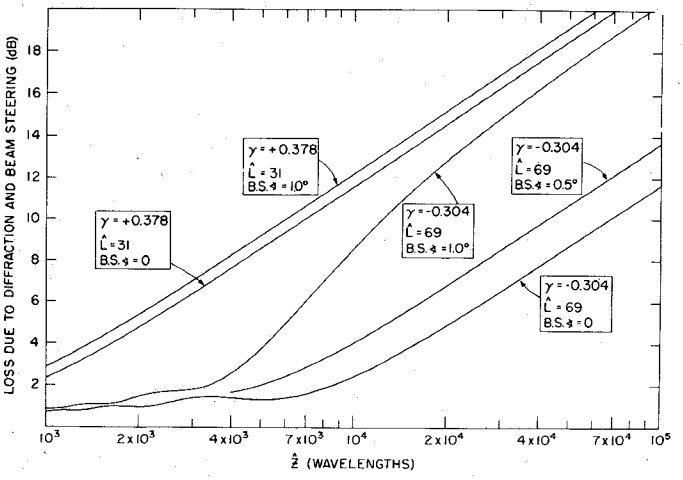

Fig. 4. Loss due to diffraction and beam steering as a function of distance in wavelengths between transducers. Value of $\gamma = +0.378$ for slope of power flow angle corresponds to ST quartz, while $\gamma = -0.304$ corresponds to 001, 110 $Bi_{12}GeO_{20}$.

design curves directly intended to aid in the choice of material. It is of interest to point out that the loss is very high for the $\hat{Z} = 75\,000$ curve near $\gamma = -1.0$. For this large distance beam steering is very important, especially for narrow undiffracted beams, and some beam spreading is to be desired. Since $\hat{Z}$ is proportional to frequency (for fixed time delay), Fig. 5 also illustrates why beam steering and diffraction are considered UHF and microwave frequency design problems. Significant losses and material tradeoff considerations exist at the higher frequencies and, of course, also for very long time delays.

Diffraction and beam steering can affect device frequency response by increasing insertion loss as a function of frequency, as shown in Fig. 6. Here $\hat{L}_0$ and $\hat{Z}_0$ represent the transducer aperture and separation at the center frequency f_0 for ST quartz ($\gamma = +0.378$) and 001, 110 $Bi_{12}GeO_{20}$ ($\gamma = -0.304$). The change in loss is slight and would be considered important only for very wide bandwidths or extreme cases (large $\hat{Z}_0$ or small $\hat{L}_0$). In general, diffraction loss decreases with frequency but propagation loss increases with frequency. These effects are partially compensating, and for certain cases it is possible to design the device so as to cancel the frequency skewing effects of these two mechanisms.

For the ST quartz case depicted in Fig. 6, the variation of all loss mechanisms will be explored in some detail in Section III.

III. OPTIMUM TRANSDUCER DESIGN

After an optimum material has been chosen, the number of interdigital periods N and the optimum acoustic aperture can be determined. In practical design situations dealing with losses and real elements, the choices of these parameters are interdependent. Thus, for example, optimum apertures should be determined for

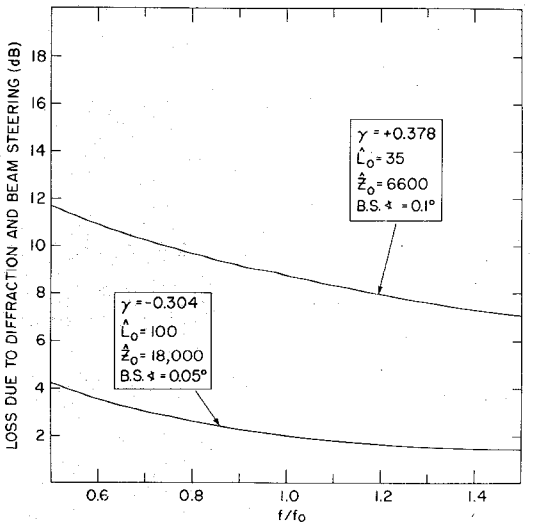

Fig. 6. Loss due to diffraction and beam steering corresponding to fixed transducer pair having an acoustic aperture at center frequency of $\hat{L}_0$, a separation at center frequency of $\hat{Z}_0$, and operated over indicated bandwidth. That is, $\hat{L} = \hat{L}_0(f/f_0)$ and $\hat{Z} = \hat{Z}_0(f/f_0)$.

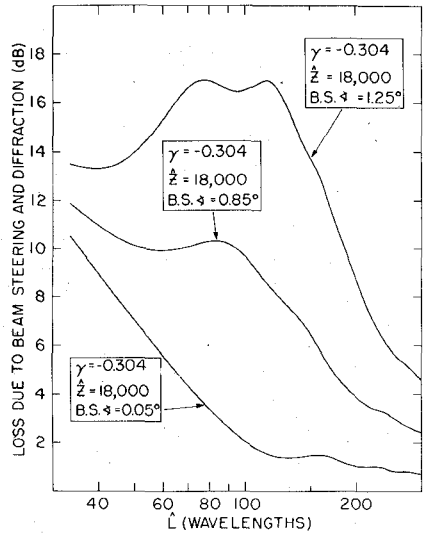

Fig. 7. Loss due to diffraction and beam steering as a function of acoustic aperture $\hat{L}$ in wavelengths. Curves correspond to 001, 110 $Bi_{12}GeO_{20}$.

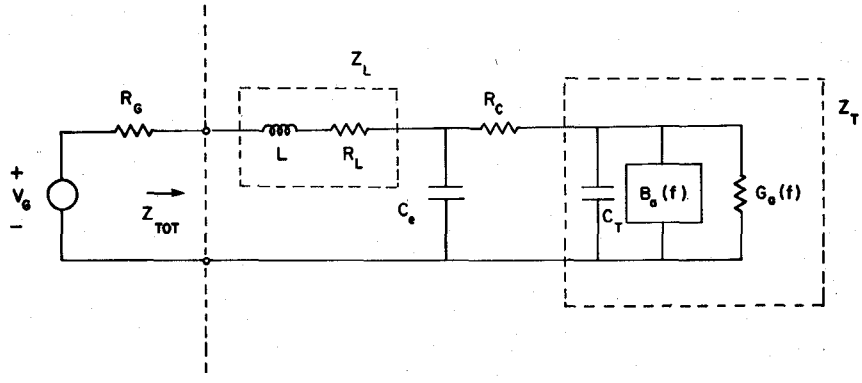

Fig. 8. Generalized equivalent circuit of periodic unapodized interdigital transducer operating in matched transmission line system. Z_T represents the usual acoustic and finger-capacitance elements, R_C represents the ohmic loss in the interdigital fingers, C_e represents parasitic shunt capacitance, and Z_L is the impedance of the lossy tuning inductor. V_G and R_G are the equivalent circuit elements of the generator.

several values of N and the absolute optimum finally chosen. A reasonable starting value for N is [10], [11]

$$N^2 = \frac{\pi}{4k^2} \tag{2}$$

where k^2 is the well-known electromechanical coupling coefficient [16]. Once the value of N is fixed, the best value of acoustic aperture depends on transducer and tuning element losses, parasitic elements, and beam steering and diffraction losses.

In order to reduce beam steering and diffraction losses it is necessary to use the widest possible acoustic apertures, as illustrated in Fig. 7. Unfortunately, electrical matching considerations limit the extent to which increased finger overlap can be used to reduce *overall* device insertion loss. To demonstrate this effect and to develop optimum delay line design procedures, it is necessary to investigate *transducer* insertion loss as a function of the various design parameters, particularly acoustic aperture. In order to accomplish this task, we adopt the generalized [12]–[14] or extended Stanford [10], [11] equivalent circuit model shown in Fig. 8, which includes lossy fingers, lossy tuning inductor, and the effects of shunt capacitance.

If only transducer effects are considered, overall delay line insertion loss in decibels is given by

$$\text{IL (dB)} = -10 \log_{10} [\text{TE}]^2 \tag{3}$$

where TE is the individual transducer efficiency [13]. Although the examples that follow used the crossed-field model, the procedures are, of course, not limited to this choice.

Neglecting propagation effects, insertion loss versus $\hat{L}$ can be directly determined using (3). Curve 3 in Fig. 9 illustrates this basic information for ST quartz and a specific set of realistic parameters [12]–[14], [17]. In addition to those parameters shown in Fig. 9, the following values corresponding to ST quartz at $f_0 = 660$ MHz were used: $N = 20$; inductor $Q = 30$; time delay $= 10$ μs, sheet resistivity [14] $\rho/t = 0.345$ $\Omega/\square$, yielding [13] a value of $R_C = 4.6$ Ω at $\hat{L} = 100$; unity finger to gap ratio and relative dielectric constant [16] $\epsilon_{PR}{}^T = 4.55$, yielding [18] a value of $C_T = 0.48$ pF at $\hat{L} = 100$; $k^2 = 0.0016$ [16]; and surface wave velocity $v_s = 3158$ m/s. The value of the tuning inductor was varied for *each* value of $\hat{L}$ to obtain the lowest value of insertion loss for that particular aperture.

When propagation loss at 660 MHz is included [8], the overall loss increases substantially, but the optimum value of acoustic aperture yielding minimum insertion loss remains the same. The final result of all our efforts is the top curve of Fig. 9, which represents the optimum design information. Beam steering and diffraction loss have been included from data similar to Fig. 7. Overall minimum insertion loss is obtained using an acoustic aperature of $\hat{L} = 100$ wavelengths. The optimum apertures were determined graphically, as this has been found to be the most convenient method in actual practice. A curve for the ideal case corresponding

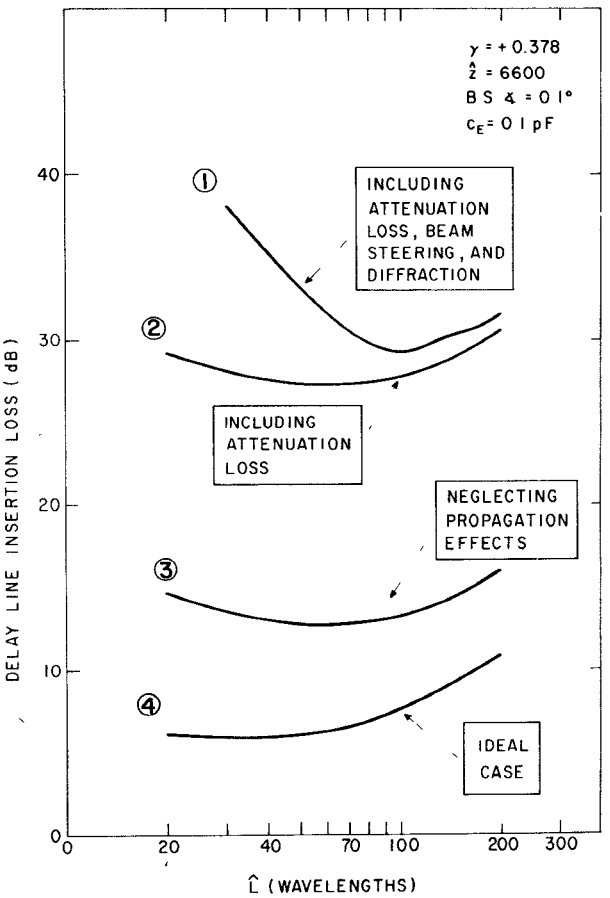

Fig. 9. Delay line insertion loss versus acoustic aperture curves used to choose optimum (minimum insertion loss) acoustic aperture Curve 1 includes real transducer effects ($Q = 30$, $\rho/t = 0.345\ \Omega/\square$, and $C_E = 0.1$ pF). attenuation loss. beam steering. and diffraction. Curve 2 includes real transducer effects and attenuation loss. Curve 3 includes real transducer effects and attenuation loss. Curve 3 includes only transducer effects. Curve 4 is the ideal case corresponding to $Q = \infty$, $\rho/t = 0$, and $C_E = 0$ with zero propagation, beam steering and diffraction losses.

to the original Stanford design procedure [10], [11] is also presented in Fig. 9 for comparison. Here, $R_L = 0$, $R_G = 0$, $C_e = 0$, BS $\not\propto = 0$, and attenuation and diffraction losses are neglected. The substantial difference is easily seen.

IV. CONCLUSIONS

Typical sets of design curves for combined beam steering and diffraction losses have been presented. These curves are expected to be particularly useful in aiding in the choice of material for any given application and in alerting the surface wave engineer as to when beam steering and diffraction become serious design constraints.

It has been shown that in the presence of beam steering, each material presents a special case and universal combined curves are not possible.

The standard design optimization procedures for determining interdigital transducer finger overlap have been extended to include beam steering and diffraction losses in addition to finger loss and external circuit effects.

REFERENCES

[1] J. J. Campbell and W. R. Jones, "A method for estimating optimal crystal cuts and propagation directions for excitation of piezoelectric surface waves," *IEEE Trans. Sonics Ultrason.*, vol. SU-15, pp. 209–217, Oct. 1968.
[2] M. B. Schulz, B. J. Matsinger, and M. G. Holland, "Temperature dependence of surface wave velocity on α-quartz," *J. Appl. Phys.*, vol. 41, pp. 2755–2765, June 1970.
[3] M. B. Schulz and M. G. Holland, "Temperature dependence of surface acoustic wave velocity in lithium tantalate," *IEEE Trans. Sonics Ultrason.*, vol. SU-19, pp. 381–384, July 1972.
[4] A. J. Slobodnik, Jr., P. H. Carr, and A. J. Budreau, "Microwave frequency acoustic surface-wave loss mechanisms on $LiNbO_3$," *J. Appl. Phys.*, vol. 41, pp. 4380–4387, Oct. 1970.
[5] A. J. Budreau and P. H. Carr, "Temperature dependence of the attenuation of microwave frequency elastic surface waves in quartz," *J. Appl. Phys.*, vol. 18, pp. 239–241, Mar. 1971.
[6] A. J. Slobodnik, Jr., and A. J. Budreau, "Acoustic surface wave loss mechanisms on $Bi_{12}GeO_{20}$ at microwave frequencies," *J. Appl. Phys.*, vol. 43, pp. 3278–3283, Aug. 1972.
[7] A. J. Slobodnik, Jr., and E. D. Conway, "The effect of beam steering on the design of microwave acoustic surface wave devices," in *Int. Microwave Symp. Dig.*, May 1970, pp. 314–318.
[8] T. L. Szabo and A. J. Slobodnik, Jr., "The effect of diffraction on the design of acoustic surface wave devices," *IEEE Trans. Sonics Ultrason.*, vol. SU-20, pp. 240–251, July 1973.
[9] I. M. Mason and E. A. Ash, "Acoustic surface-wave beam diffraction on anisotropic substates," *J. Appl. Phys.*, vol. 42, pp. 5343–5351, Dec. 1971.
[10] W. R. Smith, H. M. Gerard, J. H. Collins, T. M. Reeder, and H. J. Shaw, "Analysis of interdigital surface wave transducers by use of an equivalent circuit model," *IEEE Trans. Microwave Theory Tech. (Special Issue on Microwave Acoustics)*, vol. MTT-17, pp. 856–864, Nov. 1969.
[11] ——, "Design of surface wave delay lines with interdigital transducers," *IEEE Trans. Microwave Theory Tech. (Special Issue on Microwave Acoustics)*, vol. MTT-17, pp. 865–783, Nov. 1969.
[12] D. B. Armstrong, "Research to develop microwave acoustic surface wave delay lines," Litton Industries, San Carlos, Calif., Final Rep. AFCRL-72-0378, June 1972.
[13] H. Gerard, M. Wauk, and R. Weglein, "Large time-bandwidth product microwave delay line," Hughes Aircraft Co., Fullerton, Calif., Tech. Rep. ECOM-03852, Oct. 1970.
[14] R. D. Weglein and E. D. Wolf, "The microwave realization of a simple surface wave filter function," in *Int. Microwave Symp. Dig.*, June 1973, pp. 120–122.
[15] A. J. Slobodnik, Jr., and T. L. Szabo, "Ultralow-diffraction acoustic-surface-wave propagation on $Bi_{12}GeO_{20}$," *Electron Lett.*, vol. 9, pp. 149–150, Mar. 1973.
[16] M. B. Schulz and J. H. Matsinger, "Rayleigh-wave electromechanical coupling constants," *Appl. Phys. Lett.*, vol. 20, pp. 367–369, May 1972.
[17] A. J. Slobodnik, Jr., "UHF and microwave frequency acoustic surface wave delay lines, I. Design." Air Force Cambridge Res. Lab., Bedford, Mass., 1973.
[18] G. W. Farnell, I. A. Cermak, P. Silvester, and S. K. Wong, "Capacitance and field distributions for interdigital surface-wave transducers," *IEEE Trans. Sonics Ultrason.*, vol. SU-17, pp. 188–195, July 1970.

Application of Microstrip Analysis to the Design of a Broad-Band Electrooptical Modulator

EIKICHI YAMASHITA, MEMBER, IEEE, KAZUHIKO ATSUKI, AND TOSHIHIKO AKAMATSU

***Abstract*—This short paper describes a proposed structure of a broad-band electrooptical modulator and an application of existing microstrip analysis programs to determine dimensions of the structure for a broad-band property. Results of numerical computations indicate that it is possible to obtain a broad-band modulator by using $LiNbO_3$ or $LiTaO_3$.**

I. INTRODUCTION

The impedance matching problem of a traveling-wave electrooptical modulator has not been solved for years, though it is an important factor in the limitation of the bandwidth of the modulator [1], [2]. Recently, a lithium tantalate traveling-wave modulator has been reported which has the characteristic impedance close to the normal 50-Ω impedance system [3]. A structural design consideration to match the light velocity and the modulation wave velocity has also been reported [4]. The satisfaction of only one of two conditions, the impedance matching and velocity matching, may not be enough to obtain a broad-band property. Perhaps, the best way is to search out a modulator structure by using a computer calculation so as to satisfy these two conditions simultaneously.

II. TRAVELING-WAVE ELECTROOPTICAL MODULATORS

One of the proposed modulator structures is shown in Fig. 1(a). Material 1 is a small electrooptical crystal to modulate laser light, material 2 and 3 dielectric, and material 4 conductor to guide

Manuscript received July 9, 1973; revised November 2, 1973. This work was supported in part by the Research Project on Laser Communications.
The authors are with the University of Electro-Communications, Chofu-shi, Tokyo, Japan.